International Journal of Science and Research (IJSR)
ISSN: 2319-7064
Impact Factor 2025: 7.089

# Electric and Optical Properties of Synthesised Nano-Phase Stannic Dioxide Semiconductor

**Sujeet Kumar[1], B. C. Rai[2]**

[1, 2]Department of Physics, College of Commerce, Arts & Science, Patliputra University Patna-800020

**Abstract:** ***Nanoparticles of stannic dioxide semiconductor were synthesized chemically, and annealed at 120°C, 150°C and 200°C. FTIR spectra showed that in the crystal, Sn—O—Sn bending vibrations band spans 419-487 $cm^{-1}$ and Sn—O asymmetric stretching spans a band of 630-640 $cm^{-1}$. The chemical composition and morphology were studied by SEM-EDS. These indicated successful synthesis. Its microstructural studies were performed and published earlier. Effect of impurity on magnetic properties were also reported. However, optical and electrical studies were done by us later, and here we report the novel observations. We measured the specific capacitance of samples by cyclic voltammetry using a three-electrode configuration at a scan rate of 10 mV $s^{-1}$, showed that the samples annealed at 150 °C and 200 °C exhibited values of 113.5 F $g^{-1}$ and 327.3 F $g^{-1}$, respectively. These values are significantly higher than approximately 1.6 F $g^{-1}$ measured under comparable electrochemical conditions, and are novel for coprecipitation method. To understand the origin of this enhancement, the structural and electronic properties of the samples were examined using UV–Visible absorption spectroscopy. The optical band gaps, determined from Tauc plots of samples at the three annealing temperatures, were observed to decrease from 4.40 eV for the sample annealed at 120 °C to 3.61 eV for the sample annealed at 200 °C. This may be due to an increase in defect states, such as oxygen vacancies, and possible modifications in crystallinity and particle size induced by annealing, microstructure and electronic structure of $SnO_2$ nanoparticles.***

**Keywords:** Stannic-dioxide nanoparticle; optical band gap; specific capacitance; Annealing Temperature

## 1. Introduction

Recent fast growth of portable electronics, electric vehicles, and renewable energy technologies has created an increasing demand for efficient and sustainable energy-storage systems. Among the available technologies, rechargeable batteries and supercapacitors have attracted considerable attention because of their complementary performance characteristics (B. E. Conway (1999); Bruce Dunn, Kamath, H., & Tarascon, J.-M. (2011); Patrice Simon, & Gogotsi, Y. (2020); John B. Goodenough, & Park, K.-S. (2013)). While batteries provide high energy density, supercapacitors offer high power density, rapid charge–discharge capability, and excellent cycling stability. Consequently, the focus goes to the development of advanced electrode materials with high specific capacitance and long-term electrochemical stability. In this context come the supercapactors with charge-storage mechanism based on either electrical double-layer capacitance (EDLC), pseudo-capacitance, or a combination of both. Electrical double-layer capacitance originates from the electrostatic accumulation of electrolyte ions at the electrode–electrolyte interface, whereas pseudo-capacitance arises from fast and reversible surface redox reactions (Conway, 1999; Simon and Gogotsi, 2008; Augustyn *et al.*, 2014). Transition-metal oxides are particularly attractive electrode materials because they can contribute significantly through pseudocapacitive charge storage while maintaining good electrochemical reversibility.

Among various transition-metal oxides, tin dioxide ($SnO_2$) has emerged as a promising multifunctional semiconductor because of its wide band gap, high chemical stability, environmental compatibility, and low cost. In addition to its applications in gas sensors, transparent conducting electrodes, lithium-ion batteries, photocatalysis, and spintronics (Rao and Müller, 2004; Yamazoe and Shimanoe, 2009; Simon and Gogotsi, 2008; Dietl, 2010), $SnO_2$ has also been investigated as an electrode material for supercapacitors. However, pristine $SnO_2$ generally exhibits relatively low electrical conductivity and limited specific capacitance, which restrict its electrochemical performance. Several approaches have been employed to overcome these limitations, including nanostructuring, morphology control, defect engineering, and transition-metal doping. Reducing the particle size to the nanometre scale substantially increases the specific surface area and shortens ion-diffusion pathways, thereby facilitating charge storage. An electronic band structure, and improved charge-transfer kinetics can collectively enhance the electrochemical performance by increasing the number of electrochemically active sites and improving electrical conductivity (Simon & Gogotsi (2020), Augustyn et al. (2014)). The temperature of annealing is another important parameter influencing the properties of nanomaterials. Appropriate thermal treatment affects crystallinity, crystallite size, lattice defects, microstrain, and optical band gap, all of which influence electron transport and electrochemical behaviour. Understanding the relationship between annealing-induced structural modifications and specific capacitance is therefore essential for optimizing the performance of $SnO_2$-based electrode materials. These changes can enhance the electrical conductivity and facilitate charge transfer at the electrode–electrolyte interface, thereby contributing to the observed increase in specific capacitance.

In the present work, $SnO_2$ nanoparticles were synthesized and annealed at different temperatures to investigate the effect of thermal treatment on their electrochemical performance. Structural evolution was examined using SEM, EDS and FTIR in this work, and confirmed other microstructures studied earlier. The electrochemical behaviour was evaluated by cyclic voltammetry (CV) using a three-electrode configuration. A significant enhancement in specific capacitance with increasing annealing temperature was observed. The optical properties were investigated using UV–Visible absorption spectroscopy. The results are discussed in terms of the correlation between annealing-induced changes

in the microstructure, optical band gap, and electrochemical properties, providing insights into the design and applications of high-performance $SnO_2$-based electrode materials for energy-storage.

## 2. Experimental Method

As reported in our earlier work (**Kumar S, et al, 2023**), a pristine sample of $SnO_2$, was prepared as follows. First of all, 0.1M solution was prepared by dissolving 3.506 g of $SnCl_4.5H_2O$ in 100ml de-ionised water at room temperature. The solution was put on a hot plate with magnetic stirrer, and warmed to 35° C under stirring. Then, aqueous Ammonia was added into it drop wise. A white precipitate was obtained (at pH around 8). It was washed and dried at annealing temperature of 120°C for 5 hours followed by natural cooling to room temperature. Thus, powdered product was collected. Samples at annealing temperatures of 150°C and 200 °C were similarly prepared. We have given doping procedure also (Figure 1 B) for further work, but have used only pristine samples as processed in Figure 1(A), in this work.

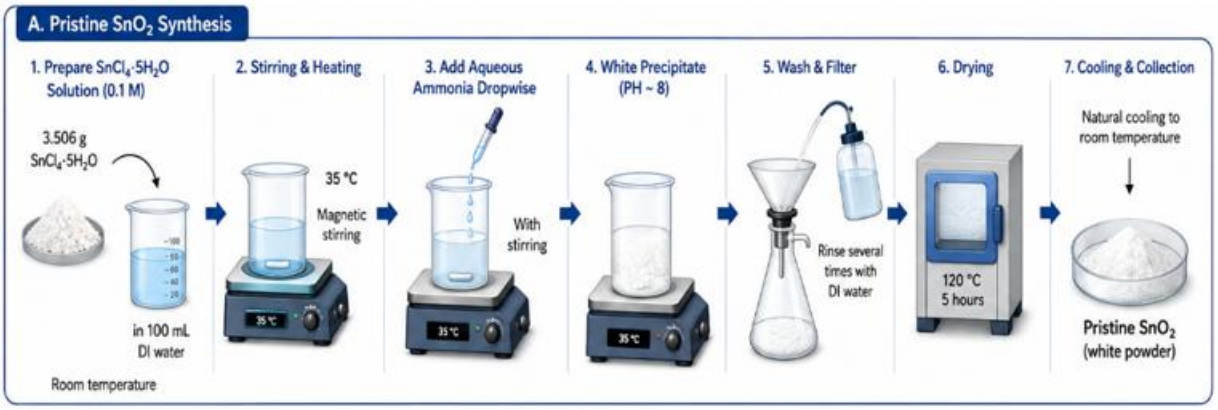


**Figure 1(A):** Synthesis Procedure for pristine samples

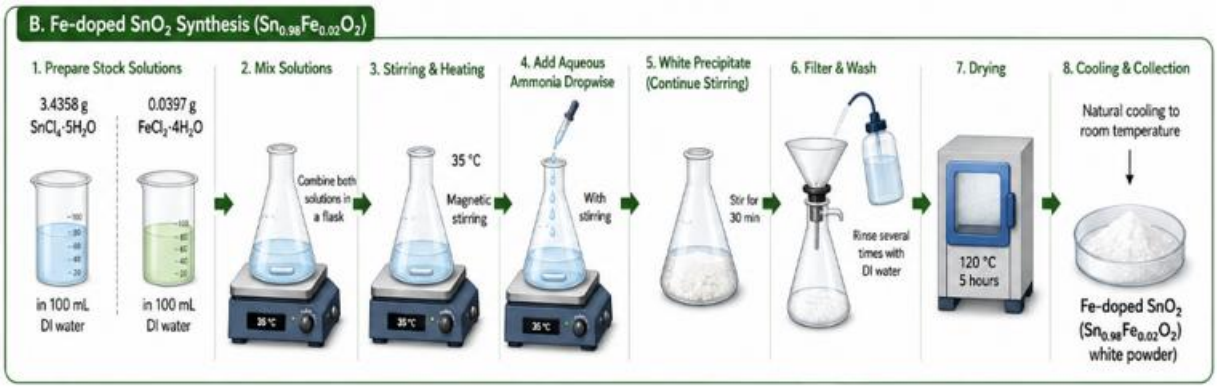


**Figure 1(B):** Synthesis of doped samples

## 3. Results and Discussions

**Structural studies: SEM and EDS**

SEM micrograms at proper magnification show morphological information. SEM Images of pristine samples synthesized show fine particles agglomerations and near-spherical morphology [Figure 2(a)]. Quantitative chemical analysis of selected area from a sample is shown in Tables [1]. The **eZAF smart quant** results show the chemical composition data, based on EDS/EDX, in usual notations.

**Table 1:** eZAF Smart Quant Results for a pristine sample

| Element | Weight % | Atomic % | Net Int. | Error % | Kratio | Z | R | A | F |
|---|---|---|---|---|---|---|---|---|---|
| O K | 13.77 | 54.23 | 120.00 | 10.39 | 0.0571 | 1.3933 | 0.7799 | 0.2976 | 1.0000 |
| SnL | 86.23 | 45.77 | 619.07 | 2.67 | 0.8385 | 0.9336 | 1.0508 | 1.0235 | 1.0178 |

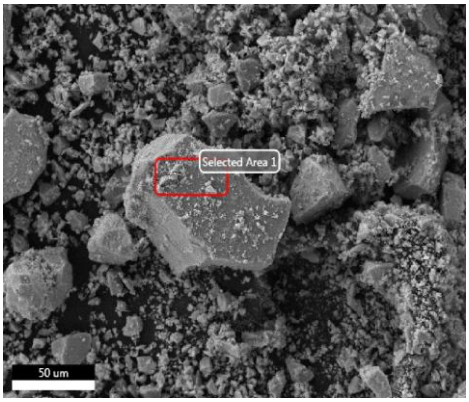


**Figure 2(a):** SEM image

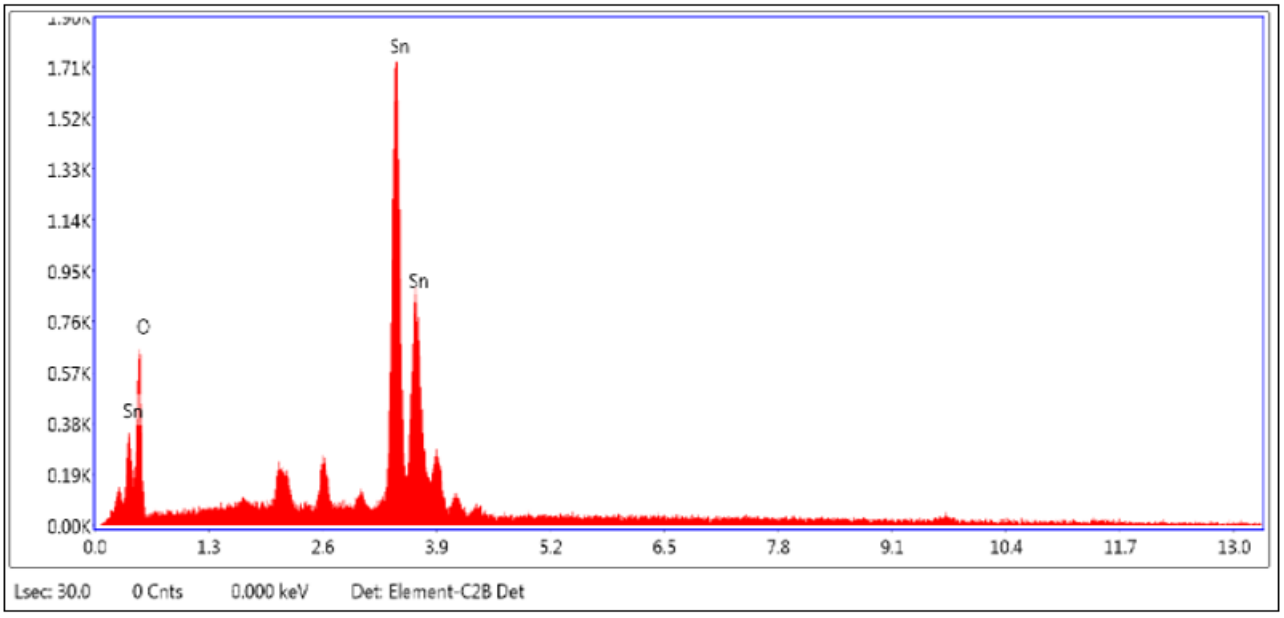


**Figure 2(b):** EDS of sample

The list of detected elements is shown as Sn, Fe and O in doped samples and Sn and O in un-doped samples. Their weight percentage, atomic percentage and correction values Z. A, F, and K-ratios are indicated [Table 1]. These confirm the formation of the envisaged compounds and their actual makeup.

**Fourier Transform Infrared Spectra:**

The chemical bonds present in a substance have vibrational energy levels that differ in wave numbers in the range of 400 $cm^{-1}$ to 4000 $cm^{-1}$[ Darr, J. A.; Zhang, J.; Makwana, N. M.; Weng, X.2019; Krušič, K. et al.,2017; El Sayed, A. M. et al.2022; Siddique, M. et al.2022]. We looked for the bonds of Sn-O, Fe-O, and chemicals used in the samples. Figure 2 (c) shows the FTIR peaks, and Table 2 shows the data for the first five peaks tabulated therein.

The spectra show that Sn—O—Sn bending vibrations are represented in rutile stannic dioxide by 419-487 $cm^{-1}$. There are variations in deep positions with concentration of Fe, attributed to amount of lattice distortion and defect generation. Wave numbers 630-640 $cm^{-1}$ show Sn—O asymmetric stretching. The Fe—O stretching vibrations lie in the band 680-750 $cm^{-1}$ (often not observed in spectrum possibly due to low concentration, but affecting the defect levels and shift in cationic energy). However, its incorporation is already shown by EDS. The Sn—OH bending or surface hydroxyl vibrations appear at weak band 940-950 $cm^{-1}$ [Harrison, P. G.; Guest, A. 1987]. Thus, the FTIR spectra confirm the bonds in synthesis of the envisaged compound.

**Electric capacitance per unit mass**

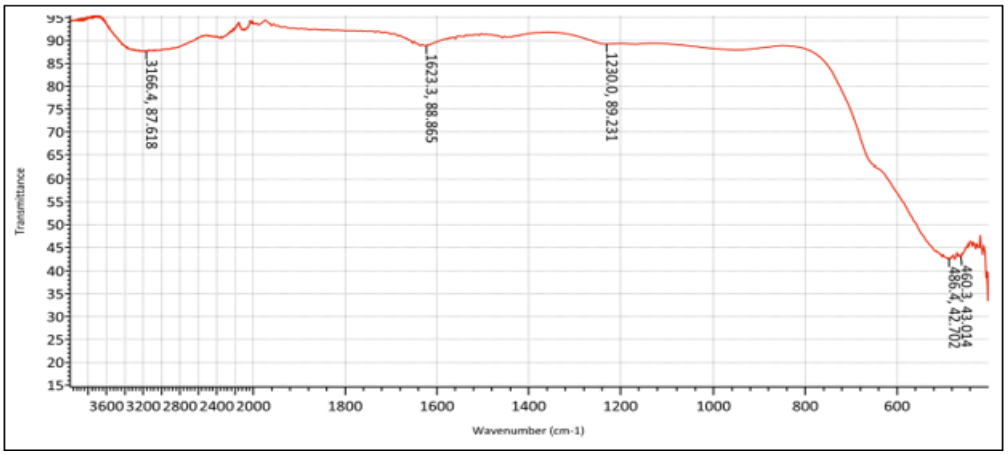


**Figure 2(c):** FTIR spectrum of sample

**Table 2:** FTIR bands in sample

| Peak Number | Wave Number ($cm^{-1}$) | Intensity |
|---|---|---|
| 1 | 460.3 | 43.014 |
| 2 | 486.4 | 42.702 |
| 3 | 1230.0 | 89.231 |
| 4 | 1623.3 | 88.865 |
| 5 | 3166.4 | 87.618 |

**Electric capacitance per unit mass:**

A three-electrode electrochemical apparatus with data acquisition system was used to measure current in working electrode and its potential relative to the reference electrode (Ag/AgCl). Each sample was subjected to three scan rates of 10 mV/s, 50mV/s and 100 mV/s. The voltammograms are displayed in Figures 3 (a through c). The specific capacitance was found to be consistent with other reports for nanoparticles and stannic dioxide nanoparticles **[Arhin D. Dodoo, et al 2018]**. It strongly depends on the content of the cell, preparation routes, annealing temperature and how fast it is scanned. If c be the specific capacitance, k the scan rate and m be the mass of the sample, the current is: $I = cmk$.

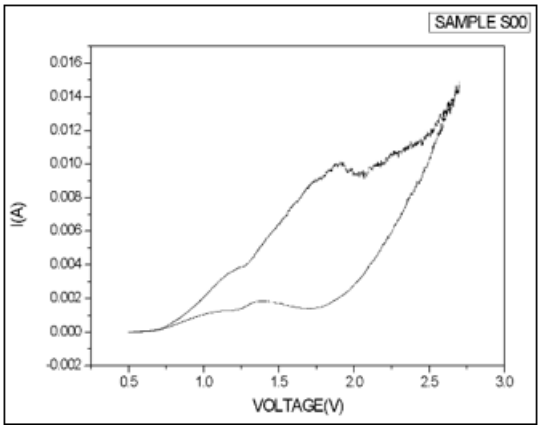


**Figure 3 (a):** I(V)-cycle of sample (annealed at 150°C) at scan rate, k= 10 mV/s

In I(V)-plot of Figure 3 (a), the current grow upon increasing the voltage from voltage $V_1$ to the maximum voltage be $V_2$. The integral I relative to V along current-voltage curve is the area under the graph, $A_1$. That is,

$$A_1 = \int_{V_1}^{V_2} IdV = cmk(V_2 - V_1)$$

In the return trip, the voltage is reduced from $V_2$ to $V_1$ along the lower curve using the same scan rate. Hence the above integral is area under the lower curve, $A_2$. The integral of current-voltage cycle is, thus, A = $A_1$ - $A_2$, so that $A = 2cmk(V_2 - V_1)$. Simplifying for c,

$$c = \frac{A}{2mk(V_2 - V_1)}$$

The area of the cycle was computed using the origin lab from the voltammogram obtained by cyclic voltammetry. Figures 3(a-c) show the experimental curves for $SnO_2$ nanoparticles, and Table 3 shows their calculated values. Three scan rates k=10 mV/s, 50 mV/s and 100 mV/s were used for each sample S00 at two annealing temperatures of 150°C and 200°C. The specific capacitance decreases with increasing scan rate [**Yu PY, Cardona M, 1996**]

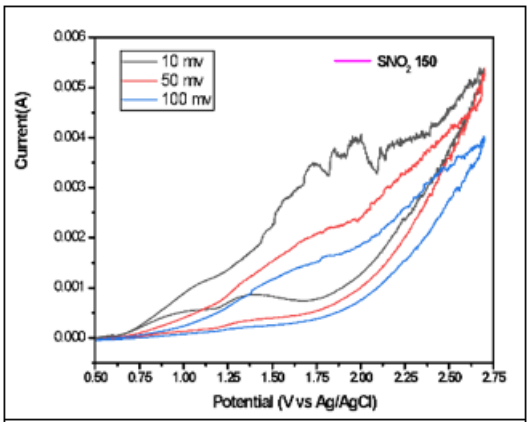


**Figure 3(b):** CV result for $SnO_2$ annealed at 150°C.

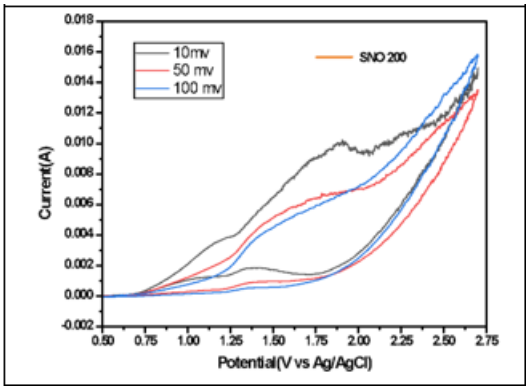


**Figure 3(c):** CV result for the sample annealed at 200°C

We observe that the specific capacitance depends on scan rates. This may be attributed to left over of microscopic details of events on fast scan rates. the specific capacitance has better values at slow rate of scan.

Also, it has greater values at greater annealing temperature: 113.5 F/g at 150ºC and 327.3 F/g at 200ºC. Possibly, better crystallinity or change in microstructure, favoured the greater specific capacitance.

**Table 3:** Calculation of specific capacitance of stannic dioxide nanoparticles

| Annealing Temp(ºC) | 150 | 200 |
|---|---|---|
| Scan rate (mV/s) | 10 | 10 |
| Sample mass (mg) | 0.5 | 0.5 |
| Area of graph (A.V) | 0.0024908 | 0.00720511 |
| V1=potential (volt) | 0.5062 | 0.49884 |
| V2= potential (volt) | 2.7005 | 2.7005 |
| **Specific Cap (F/g)** | **113.512** | **327.258** |
| Potential window(V) | 2.1943 | 2.20166 |

In literature, pure $SnO_2$ nanoparticles synthesized by precipitation or sol–gel process, a specific capacitance in the range of 120–250 F $g^{-1}$ is typical. Higher values (400–500 F $g^{-1}$) are generally achieved with optimized porous nanostructures, high surface area, or conductive supports [M. N. M. Makwana *et al.* (2023); Wang L P. et al. (2017)].

**Optical Properties**

Absorption of radiation falling on a sample was studied using ultraviolet and visible radiation in the range (200 nm-800nm). Figure 4 (a) shows that $SnO_2$ (200ºC) sample exposed to the radiations shows high transmission in low wavelengths and high absorption in higher wavelengths

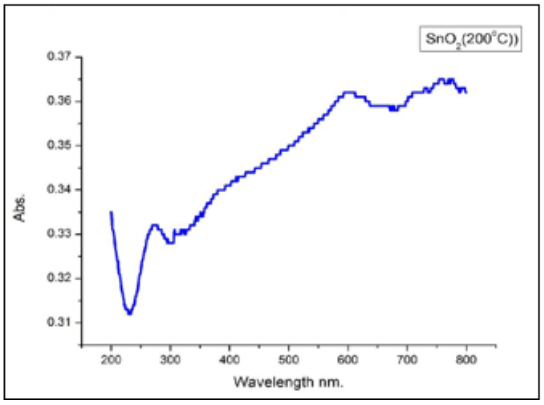


**Figure 4 (a):** Absorbance versus wavelength plot

Absorbance –wavelength data were used to study inter-band transitions, and band gaps were calculated for samples at different annealing temperatures [Figures 4(b)]. Optical band gap in terms of incident photon energy and absorption coefficient is given by

$$(\alpha h\nu)^n = B(h\nu - E_o)$$

This is Tauc's equation and its graphical representation is called Tauc's plot [ **Tauc J, 1966;1968**]. The parameter B is probability parameter of inter-band transition, and index n depends upon nature of the band gap transitions: 2 for allowed direct transition, ½ for allowed indirect transitions; 2/3 for forbidden direct transition and 1/3 for forbidden indirect transitions. In direct band gap $SnO_2$, we take n=2.

The linear part of the Tauc's plot against photon energy in Figures 4(b) extends to intersect abscissa at the optical band gap, Eo. Table 4 shows the values of band gaps for different annealing temperatures of our samples.

**Table 4: Optical band gaps of samples at different temperatures**

| Sample | Annealing Temperature (ºC) | Optical band gap (eV) |
|---|---|---|
| S1 | 120 | 4.4 |
| S2 | 150 | 4.2 |
| S3 | 200 | 3.61 |

As the annealing temperature increases, the band gap decreases. Such a behaviour is also reported by [**Abebe G. Habte, et al, 2019**]. This may be attributed to improved crystallinity and reduced strain **[Rani N, Jaggi N, 2020; Hamed A G, 2017**].

One may notice the systematics shown in the graphs as annealing temperature is changed. At higher temperature, better crystallinity is expected, and optical band gap slightly decreased from 4.4 eV to 3.61 eV as the annealing temperature increased from 120ºC to 200ºC. The Brus quantum confinement model explains the decrease in the optical band gap with increasing annealing temperature[**Brus, L. 1986**]. The Brus equation, in usual notations, reads

$$E_g = E_g^{bulk} + \frac{\hbar^2\pi^2}{2r^2}\left(\frac{1}{m_e} + \frac{1}{m_h}\right) - \frac{1.8e^2}{4\pi\epsilon_0\epsilon_r r}$$

Higher annealing temperatures promote crystallite growth, resulting in an increase in particle size, r, and a reduction in quantum confinement effects. As the particle size approaches the bulk regime, the confinement energy decreases, leading to a gradual narrowing of the optical band gap. Furthermore, improved crystallinity and a reduction in lattice

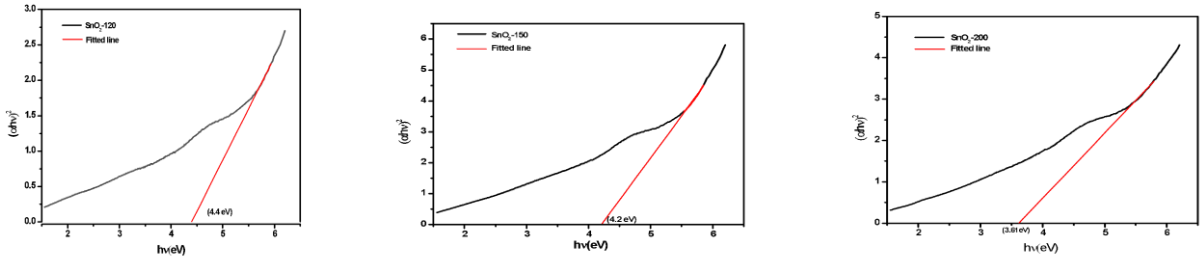


**Figure 4(b):** Optical Band Gaps of samples annealed at 120ºC, 150ºC and 200ºC

defects contribute to the observed band-gap narrowing. Therefore, the decrease in band gap observed in $SnO_2$ nanoparticles with increasing annealing temperature is consistent with the Brus model, provided that the increase in crystallite size is confirmed by x-ray diffraction analysis.

## 4. Conclusion

Electric and optical properties of nano-phase pure samples of stannic dioxide studied for their control by annealing temperature.

SEM-EDS studies revealed correct elemental composition of samples prepared, Sn and O in $SnO_2$ sample, and no other elements, as also observed in [**Preethi T, et al., 2022**]. FTIR also revealed metal-oxide bond formation correctly.

For these samples, electrical capacitance per unit mass measured by CV instrument lies in the range of orders reported in literature. It depends upon scan rate and sample synthesis procedure, and found usually greater than 1.6 F/g [**Arhin D. Dodoo et al, 2018**]. Observed values of 327 F/g for sample annealed at 200°C and 113 F/g for 150°C show dependence on annealing temperature, and are much larger than 1.6 F/g, The I-V-loops exhibit different shapes than usual duck, because of different rates of redox reactions in rising and falling portions of potential profile applied.

To investigate the effect of annealing temperature on nanostructure, optical band gap was measured by Tauc's plots for different annealing temperatures. The observed band gaps show a blue shift relative to bulk, which is a feature of quantum confinement. The values found are 3.61, 4.2 and 4.4 eV corresponding to temperatures of annealing 200°C, 150°C and 120° C, which shows a nice pattern of crystallinity [**Abebe G. Habte, et al, 2019; Rani N, Jaggi N, 2020; Hamed A G, 2017].** Finally**,** annealing-induced changes in the microstructure of samples control the optical band gap and electrochemical properties, opening scope of high-performance $SnO_2$-based electrode materials for energy-storage applications.

**Acknowledgement**
Authors are grateful to faculties of Physics Departments of Patliputra University and Patna University, and Centre of Nanoscience and Nanotechnology, Aryabhata Knowledge University, Patna for their academic support. *The work was not funded by any organization, and authors declare that they have no conflict and competing interest in publishing the work.*

## References

[1] Abebe G. Habte, Fekadu G. Hone, Francis B. Dejene, *Journal pre-proof Physica B: Physics of condensed matter* ,2019; 7: p. 411760.
[2] Arhin D. Dodoo, R.A. Nuamab, P.K. Jain, D.O. Obada, A.yaya*, Result in Physics* ,2018; 9:p.p. 1391-1402.
[3] B. E. Conway (1999). Electrochemical Supercapacitors: Scientific Fundamentals and Technological Applications**.** Kluwer Academic/Plenum Publishers.
[4] Bruce Dunn, Kamath, H., & Tarascon, J.-M. (2011). Electrical Energy Storage for the Grid: A Battery of Choices**.** *Science*, **334**(6058), 928–935. https://doi.org/10.1126/science.1212741
[5] Brus, L. E. *"Electronic wave functions in semiconductor clusters: experiment and theory." Journal of Physical Chemistry*, **90** (12), 2555–2560 (1986).
[6] C. N. R. Rao, & Müller, A. (Eds.). (2004). The Chemistry of Nanomaterials: Synthesis, Properties and Applications**.**Wiley-VCH. *Application:* General properties and applications of $SnO_2$ nanomaterials.
[7] Darr, J. A.; Zhang, J.; Makwana, N. M.; Weng, X. *One-Step Synthesis, Structure, and Band Gap Properties of $SnO_2$ Nanoparticles Made by a Low Temperature Nonaqueous Sol–Gel Technique.* **ACS Omega**, **2019**, *4*(2), 3643–3653.
[8] El Sayed, A. M. et al. *Design of $SnO_2$:Ni,Ir Nanoparticulate Photoelectrodes for Efficient Photoelectrochemical Water Splitting.* **Nanomaterials**, **2022**, *12*, 657.
[9] Hamed A Gatea, "Impact of Sintering Temperature on Crystallite size and Optical Properties of SnO2 Nanoparticles",2nd AiCIS, 2020 IOP Publishing, JOP: Conference Series, 1829(2017), p. 012030.
[10] Harrison, P. G.; Guest, A**.** *Tin oxide surfaces. Part 17—An infrared and thermogravimetric analysis of the thermal dehydration of tin (IV) oxide gel. Journal of the Chemical Society, Faraday Transactions 1*, **1987**, 83, 3383–3397.
[11] John B. Goodenough, & Park, K.-S. (2013). The Li-Ion Rechargeable Battery: A Perspective**.** *Journal of the American Chemical Society*, **135**, 1167–1176. https://doi.org/10.1021/ja3091438
[12] Krušič, K. et al. *$SnO_2$ Nanostructures: Effect of Processing Parameters on Their Structural and Functional Properties.* Nanoscale Research Letters, 2017, *12*, 254.
[13] Kumar S. et al. (2023), Microstructural and magnetic properties of nano phase Iron-doped stannic Oxide semiconductor synthesized for spintronics Applications, Bulletin of Pure and Applied Science Physics, 42(2), 70-74.
[14] L. Brus, (1986) Electronic wave functions in semiconductor clusters: experiment and theory, J. Phys. Chem., 90, 2555-2560
[15] M. N. M. Makwana *et al.* (2023). Microwave-assisted fabrication of $SnO_2$ nanostructures as electrode for high-performance pseudocapacitors. *Journal of Energy Storage*, 59, 106358.
[16] https://doi.org/10.1016/j.est.2022.106358
[17] Norio Yamazoe, & Shimanoe, K. (2009). **Theory of power laws for semiconductor gas sensors.** *Sensors and Actuators B: Chemical*, **138**, 100–107.
[18] Patrice Simon, & Gogotsi, Y. (2020). Perspectives for electrochemical capacitors and related devices**.** *Nature Materials*, **19**, 1151–1163. https://doi.org/10.1038/s41563-020-0747-z
[19] Patrice Simon, & Yury Gogotsi (2008). Materials for electrochemical capacitors**.** *Nature Materials*, **7**, 845–854. https://doi.org/10.1038/nmat2297
[20] Preethi T, K.Senthil, and Stefano Bellucci et al. *Saga Journals Adsorption Science & Technology*, 2022; 2022

[21] Rani Nirmala and Jaggi Neena, *Bull Mater Sci* 2020; 43:146
[22] Siddique, M. et al. *A Reliable Chemiresistive Sensor of Nickel-Doped Tin Oxide (Ni–$SnO_2$) for Sensing Carbon Dioxide Gas and Humidity.* Scientific Reports, 2022.
[23] Tauc, J. "Optical properties and electronic structure of amorphous Ge and Si", *Materials Research Bulletin*, 1968; 3:37-46 doi:10.1016/0025-5408(68)90023-8.;
[24] Tauc, J., Grigorovici, R., & Vancu, A. (1966). *Optical Properties and Electronic Structure of Amorphous Germanium*. Physica Status Solidi (b), 15, 627–637.
[25] Tomasz Dietl (2010). A ten-year perspective on dilute magnetic semiconductors and oxides.
[26] *Nature Materials*, **9**, 965–974.
[27] V. Augustyn, Simon, P., & Dunn, B. (2014). Pseudocapacitive oxide materials for high-rate electrochemical energy storage**.** *Energy & Environmental Science*, **7**, 1597–1614.
[28] https://doi.org/10.1039/C3EE44164D
[29] Wang L P. et al. (2017), Novel Preparation of N-doped $SnO_2$ Nanoparticles via Lasser – Assisted Pyrolysis: Demonstration of Exceptional Lithium Storage properties, Adv. Mater. 29(6), 1603286
[30] Yu, P.Y., Cardona M.," Fundamental of Semiconductors*", Springer, Berlin.* 1996; ISBN 3-54061461-3.